3rd Specialty Conference on Disaster Prevention and Mitigation
3e Conférence spécialisée sur la prévention et la mitigation des désastres naturels

Montréal, Québec
May 29 to June 1, 2013 / *29 mai au 1 juin 2013*

Effect of relative orientation on the capacity of a transmission tower under downburst loading

T.G. Mara[1] and H.P. Hong[2]
[1]Ph.D. Candidate, Department of Civil and Environmental Engineering, University of Western Ontario
[2]Professor, Department of Civil and Environmental Engineering, University of Western Ontario

Abstract: The wind speed profile over the height of a structure in high intensity wind (HIW) events, such as downbursts, differs from that associated with traditional atmospheric boundary layer (ABL) winds. Current design codes for lattice transmission towers contain only limited advice on HIW, and structural design is often carried out using a procedure developed for ABL winds. Furthermore, the load effects due to the relative orientation of a tower to HIW event are not well understood. The present study assesses the yield and maximum capacity of a self-supported transmission tower under downburst outflow winds, including the effects of material and geometric nonlinear behaviour. The force-deformation relationship, also known as a capacity curve, for the tower is obtained for a range of wind directions and represents the relationship between the base shear of the tower and the displacement of the tip. The capacity curve of a tower is a convenient way to assess a tower design under HIW, as the definition of a reference wind speed between downburst events is challenging due to number of parameters affecting the downburst wind profile. Capacity curves based on two downburst scenarios are obtained for oblique wind directions, and their differences are shown to be related to the shape of the loading profile, and therefore the size of the downburst. It is shown that the lowest yield capacity tends to occur at a wind direction of approximately 45°, and that the tower has a greater capacity when the loading is concentrated at mid-height as opposed to the upper portion.

1 Introduction

Transmission structures play an important role in the efficient transmission and distribution of electricity across great distances. Extreme wind events are the most common cause of failure or collapse, which includes strong synoptic events (e.g., strong winds during a wind storm) and localized high intensity wind (HIW) events, which are usually attributed to convection (e.g., thunderstorm gust front, downburst outflow). These winds differ in both meteorological and structural loading characteristics, however each of them exert great loads on transmission structures. An example of this was the failure of 19 towers in the southern portion of the Manitoba Hydro power transmission corridor due to multiple downburst events (McCarthy and Melsness 1996). Some locations in Manitoba were without power for as much as 5 days following these failures. In light of this event, an initiative was taken to better understand the characteristics and mechanisms of HIWs (Hangan et al. 2008, Banik et al. 2008), their load effects on towers (Mara et al. 2010, Lin et al. 2012), and the response of transmission structures under downburst (Shehata and El Damatty 2008, Banik et al. 2010, Darwish and El Damatty 2011).

The term ‘downburst’ was coined by Fujita (1976) to describe a strong convective downdraft which impinges on the surface of the earth, resulting in an outburst of strong winds close to ground level. The second characteristic, strong winds close to ground level, makes them especially important to man-made

structures. Due to their relative rarity and localized nature, it is uncommon to observe a downburst event at full scale, let alone have wind speed measurement devices in place to record data. A rare exception to this is the microburst captured at Andrews Air Force Base on 1 August 1983 (see Fujita 1985), which indicates a peak wind speed of approximately 67 m/s (130+ kts) at a height of 4.9 m on the leading side of the outflow. This is a benchmark observation which illustrated that downbursts are capable of generating extreme winds close to ground level, and provided a magnitude to consider along with past forensic damage surveys.

Due to the paucity of full scale downburst data, most work in the wind engineering community has proceeded by adopting a numerical approach to modelling downburst winds, while using the few recorded full scale events (Fujita 1985, Orwig and Schroeder 2007) for model calibration and validation. A numerical downburst simulation based on a stationary impinging jet was carried out by Hangan et al. (2003), and was shown to agree well with full scale downburst wind speed measurements (Kim and Hangan 2007). This is a benchmark simulation, as it provided the first spatio-temporal downburst outflow model which could be applied to structures. The numerical downburst wind fields generated by Hangan et al. (2003) are used in the present study.

It is important to note that, unlike for atmospheric boundary layer (ABL) winds where the mean wind speed profile increases monotonically over the height of the tower and is constant in time and space, the wind speed profile in a downburst outflow varies with downburst size, position (relative to a fixed structure), and time. Thus, the wind speed profile experienced by a fixed structure is transient. This complicates a practical definition of a height at which to reference the strength of downburst wind speeds, which has implications for codified design. Therefore, a simplification of design verification for structures under downburst wind loading is worth exploring. One approach that can be taken is the use of the nonlinear static pushover (NSP) method, which was used to evaluate the capacity of a 2-D transmission tower under a variety of wind loading conditions by Banik et al. (2010). It was shown that the capacities of the tower at the incipient of yield and collapse are influenced by the shape of the wind speed profile over the height of the tower. More importantly, it was shown that the capacities estimated through the NSP method are representative of the peak effects of short-duration winds, for example 3-second gusts. As the failure of a tower depends directly on the behaviour of its force-deformation relationship, or capacity curve, the evaluation of these capacities are of importance to assessment and design.

2 Modelling of transmission tower and wind loads

2.1 Numerical model of transmission tower

The effects of downburst winds are assessed for a self-supported lattice transmission tower design provided by Manitoba Hydro. The commercial finite element analysis program ANSYS® was selected for its capability in dealing with the nonlinear geometric and material properties of the structural steel of the tower. The tower members are modelled as 2-node nonlinear 3-D frame elements, assuming that rigid connections are representative of the multi-bolted moment-resisting connections found in the prototype. The masses of the conductors and ground wires are applied to the tower as lumped masses at the nodes corresponding to connections. The material nonlinearity of the tower members is modelled using bilinear elastoplastic material properties, and the geometric nonlinearities (i.e., buckling effects) are accounted for through a large deformation analysis. A total of 959 elements and 405 nodes are used in the numerical model of the tower, and a 3-D view tower model is shown in Figure 1.

2.2 Wind load provisions in codes

Design wind loads for transmission towers under synoptic winds are specified in CAN/CSA C22.3 No. 60826-10 (referred to hereafter as CSA-2010) (CAN/CSA 2010), as well as ASCE Manual No. 74 (referred to herein as ASCE-74) (ASCE 2010). CSA-2010 adopts the International Electrotechnical Commission (IEC) Standard 60826:2003 (IEC 2003) for design criteria of overhead transmission lines. The loading application used here reflects that recommended in CSA-2010.

The prototype tower is divided into 11 representative sections, or loading panels, over which the aerodynamic parameters do not significantly change. As transmission structures are often located in open terrain, an exposure representative of open country (as specified in CSA-2010) is considered, which corresponds to a power law coefficient of 0.16 for mean wind speed. It should be noted that the CSA-2010 reference wind speed corresponds to a 10-minute mean wind speed at 10 m height in open country terrain.

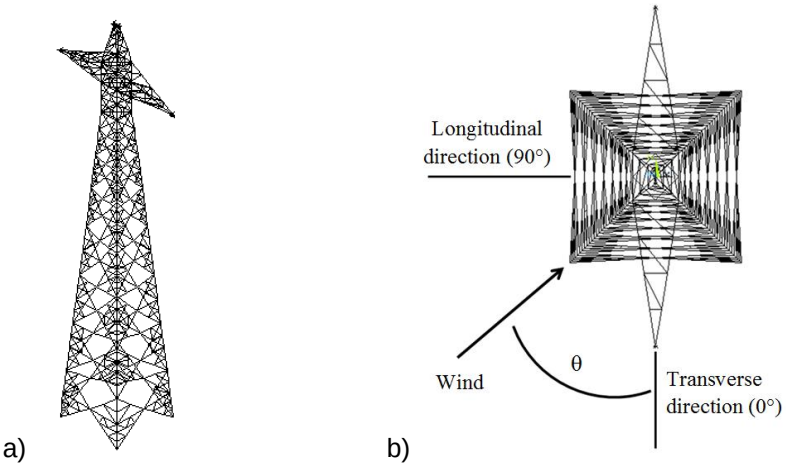

Figure 1. Self-supported transmission tower in a) isometric elevation view and b) plan view

In accordance with CSA-2010, the wind load on a single panel is calculated as

[1] $A_t = 0.5\tau\mu V_R^2 G_t(1+0.2\sin^2(2\theta))(S_{t1}C_{xt1}\cos^2\theta+S_{t2}C_{xt2}\sin^2\theta)$

where A_t (N) is the total wind load on the panel in the direction of the wind; τ is an air density correction factor taken to be 1; μ is the density of air taken to be 1.225 kg/m^3; V_R (m/s) is the reference wind speed at 10 m height based on a 10-minute averaging period in open country terrain; θ is the angle of attack of the wind (as illustrated in Figure 1); S_{t1} and S_{t2} (m^2) are the total surface areas projected normally on the corresponding faces 1 and 2; C_{xt1} and C_{xt2} are the drag coefficients for the corresponding faces 1 and 2, and; G_t is the combined wind factor accounting for the roughness of the terrain and height of the panel. In this case, faces 1 and 2 correspond to the transverse and longitudinal faces of the tower, respectively.

The wind load on the conductor and ground wire lines are calculated as

[2] $A_c = 0.5\tau\mu V_R^2 G_c G_L d L C_{xc}\sin^2\Omega$

where A_c (N) is the total wind load on the wire; C_{xc} is the drag coefficient of the wire taken to be 1; G_c is a combined wind factor accounting for the roughness of the terrain and the height of the wire; G_L is a span reduction factor based on the length of the span; d (m) is the diameter of the wire; L (m) is the wind span of the wire, and; Ω is the angle of attack between the wind direction and the wires. Note that if there is no line angle between consecutive towers (i.e., tangent towers), Ω is equal to (90-θ)°. As there are no commonly accepted equations available for the evaluation of wind loads under downburst, Eqs. [1] and [2] are used in conjunction with a simulated downburst wind profile over the height of the tower. The simulated downburst wind profiles are described in detail in the following section.

2.3 Downburst wind loads

Downbursts are characterized by strong winds at low levels, which are a result of a cool mass of air descending from the upper atmosphere impinging on the surface of the earth. This results in an outflow radiating outwards from the center of downburst touchdown. The spatio-temporally varying wind fields simulated by Hangan et al. (2003) were obtained and processed, and the simulated downburst wind field

defined by Kim and Hangan (2007) is used in this study. The downburst wind field is characterized by the jet diameter, D_{jet}, the jet velocity, V_{jet}, and the distance from touchdown to the point of interest, r. Based on these parameters, a horizontal wind profile having speeds V_{hor} is defined. As the spatial characteristics of the simulated wind fields are a function of r and D_{jet}, it is convenient to express the distance from touchdown to the point on interest as r/D_{jet}. The magnitude of the wind speeds are a function of V_{jet}. The parameters relevant to the downburst simulation are shown in Figure 2.

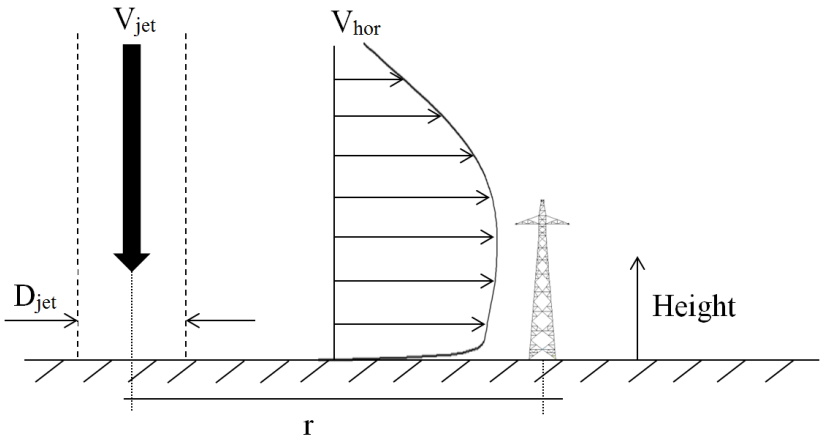

Figure 2. Elevation view of tower showing downburst touchdown and outflow (profile scale relative to downburst having D_{jet} = 500 m)

The simulated downburst outflow profiles over the height of the tower are used to evaluate the response to downburst wind loading. It was found from the simulated wind fields that the strongest horizontal wind speed occurs at a distance from touchdown of r/D_{jet} = 1.3 at the (simulation) time step 31. This time step in the downburst outflow provides the base configuration for comparison of the response of the tower under downburst winds to that under ABL and rectangular winds. Based on this position (r/D_{jet}) and time step of the outflow, the wind profile over the height of the structure is extracted and plotted in Figure 3 for various downburst sizes.

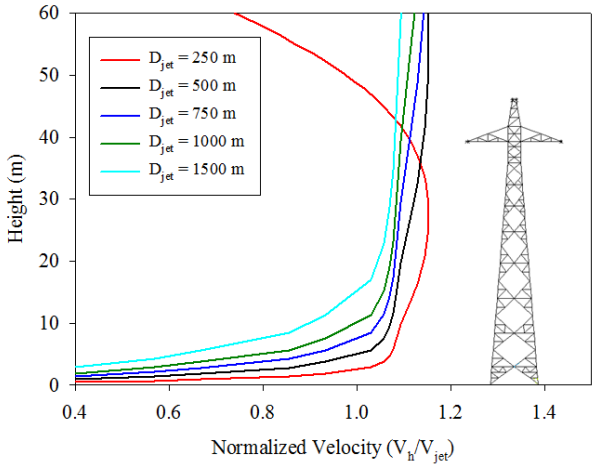

Figure 3. Downburst profiles for varying D_{jet} with tower shown for scale

In each analysis case, the response of the tower corresponds to the time step at which the peak outflow wind speed is acting on the tower structure. The parameters corresponding to the downburst acting on the tower is described as $(r/D_{jet})_T$. The wind loads on the wires vary with wind direction and downburst location, and the distance between any point i on the wire is described by $(r/D_{jet})_{Ci}$. The contributions of

the wind on the wires were considered over half the wind span from the tower of interest, which is a span of 244 m. This sign convention is shown in Figure 4, which is not to scale in order to show the details of tower and wires.

As the wind profile during a downburst is heavily dependent on the size of the downburst, D_{jet}, the profiles corresponding to several D_{jet} are shown in Figure 3. The results presented later in the paper focus on two downburst scenarios: Scenario 1 is defined by a D_{jet} of 250 m at $(r/D_{jet})_T = 1.3$, and; Scenario 2 is defined by a D_{jet} of 1000 m at $(r/D_{jet})_T = 1.3$. The wind profiles for each location i along the wires are taken from the wind profiles at the spacing intervals of the numerical simulation. For example, for downburst scenario 1 at $\theta = 0°$, $(r/D_{jet})_T = 1.3$ while $(r/D_{jet})_{Ci}$ at mid-span = 1.6; this results in a lower wind speed on portions of the wires away from the tower. The same value of $(r/D_{jet})_{Ci}$ is used for each set of wires (windward conductors and leeward conductors), as their separation is negligible compared to the spatial dimensions of the downburst.

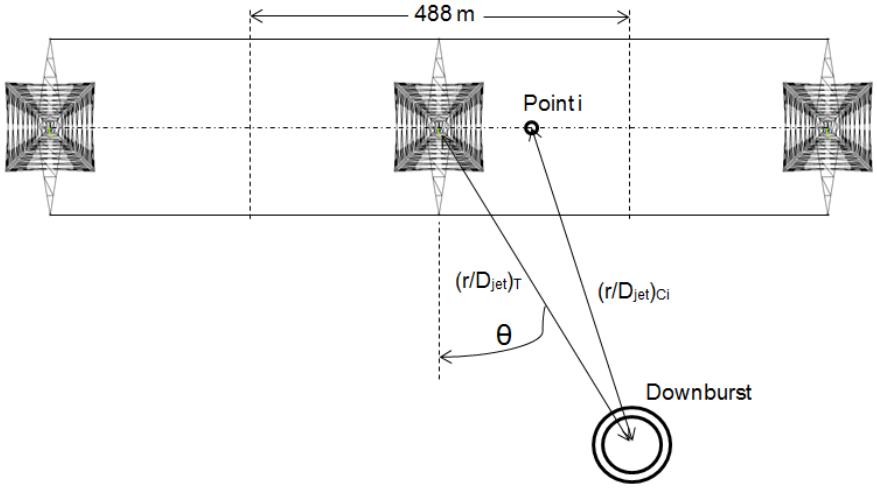

Figure 4. Plot of transmission tower and lines showing the naming convention for downburst profiles used in the analysis

3 Capacity curves for the transmission tower

3.1 Capacity curves using the NSP method

The NSP method is a widely used analysis technique to evaluate the performance and capacity of structures under seismic loading (e.g., Krawinkler and Seneviratna 1998), and more recently has been used for horizontal point load (Lee and McClure 2007) and wind load (Banik et al. 2010) applications. Banik et al. (2010) showed that the capacity curve obtained using the NSP method provides a good approximation of that obtained through using a nonlinear incremental dynamic analysis, and that the capacity curves developed represent the peak wind load effects on the structure. Therefore, the responses of the tower can be viewed as representative of the peak wind load effects for short-duration (i.e., 3-second gust) wind speeds. Through the NSP method, the applied forces are monotonically increased, while a constant loading profile, in this case a wind loading profile, is maintained. An example capacity curve for a nonlinear inelastic system is shown in Figure 5.

The NSP method is applied here to evaluate the capacity curve of the tower, which identifies the yield and maximum (or ultimate) capacities of the tower. The capacity curves presented reflect the relationship of the total applied horizontal wind load to the displacement of the tip of the tower. The total applied horizontal wind load equals the base shear if it is assumed that inertial forces are negligible. The capacity curves are approximated as a bilinear system to estimate the yield capacity, which is defined as the point of intersection of the tangents to the elastic and post-yield behaviour (as indicated in Figure 5). The

maximum capacity is defined by the incipient of collapse of the tower, which is the point of nonconvergence in the numerical model. Mean values of the structural material properties and geometric variables as supplied by Manitoba Hydro are used for the evaluation of the capacity curves.

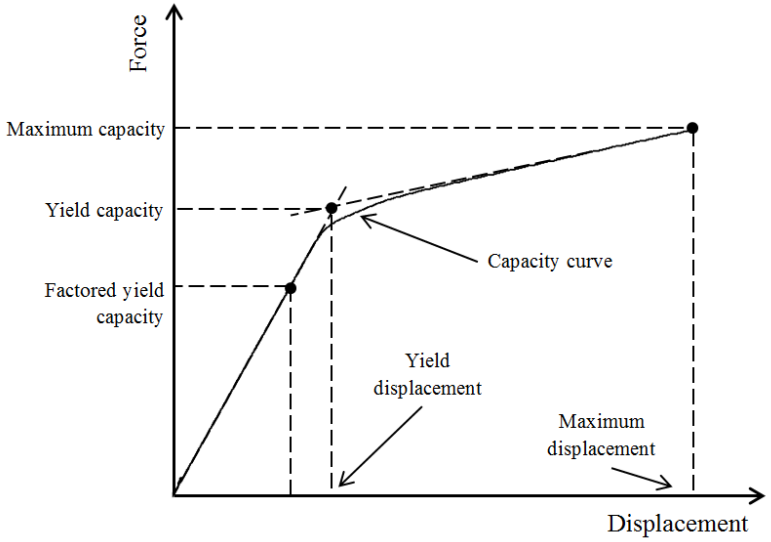

Figure 5. Example capacity curve for a nonlinear inelastic system

3.2 Capacity curves for downburst wind profiles

The capacity curves for downburst scenario 1 (DB1) and downburst scenario 2 (DB2) are evaluated for 11 wind directions: 0° (transverse direction), 90° (longitudinal direction), and at increments of 10° in between, as well as for wind at 45°. The downburst wind profiles for each downburst scenario are evaluated using the methodology described in Section 2.3. The NSP method is used to carry out the analysis for each downburst scenario, and the obtained capacity curves are shown for selected wind directions in Figure 6. It is shown that for DB1, which is characterized by the strongest winds over the mid-height of the tower (see Figure 3), the yield capacity is the lowest for wind at 45°. Also note that the capacity curve for wind at 45° is lower than for any other wind direction. The yield capacities for wind at 30° and wind at 60° fall between their respective adjacent yield capacities, which is expected due to the loading relationship between wind directions (see Eqs. [1] and [2]).

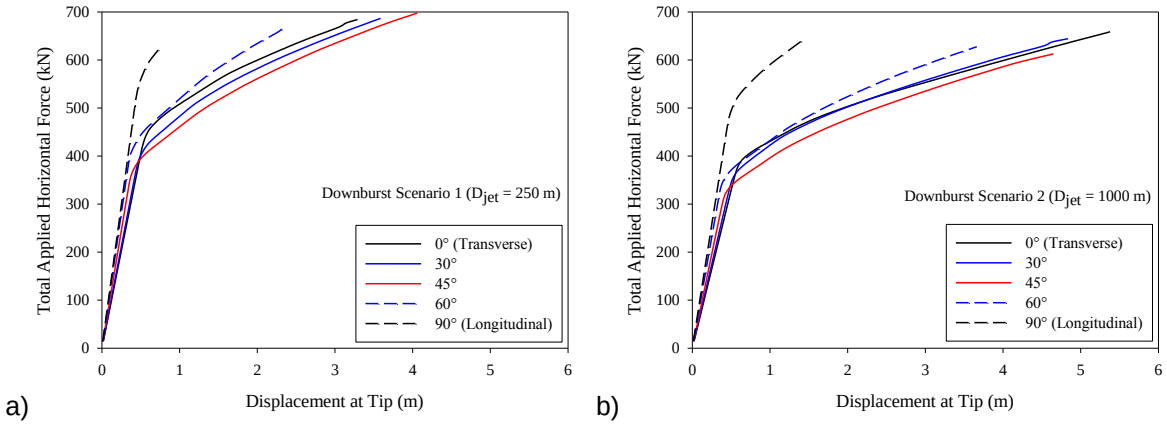

Figure 6. Capacity curves for selected wind directions for a) downburst scenario 1 and b) downburst scenario 2

The capacity curves for DB2 are characterized by lower yield capacity and greater post-yield deformation when compared to those for DB1. This is true even for wind at 90°, where there is significantly more post-yield deflection than was observed for DB1. In each case, this is due to the loading distribution of DB1 having a greater impact in the upper portion of the tower. For the transverse direction, the greater wind load at the top of the tower is important as the wires are in this zone, which results in the relatively large amount of post-yield deformation. The same effect is shown for the longitudinal direction due to the asymmetry of the tower cross-arm, but to a lesser extent as the cross-arm feature does not impact the overall load as much as the wires (and the wires are not loaded for wind at 90°). Similarly to DB1, the lowest yield capacity was observed for wind directions in the 45° - 50° range, and the yield capacity at the other wind directions are in approximately the same ratio as those for DB1. That is, the yield capacities for different wind directions follow similar trends between downburst sizes. The maximum capacity is shown to be lower for DB2 for each wind direction except for wind at 90°, and this is again attributed to the increased loading on the wires with respect to the rest of the tower. The capacity curve for wind at 60° follows that for wind at 90° closely in the elastic range, which implies that the loading on the wires does not have much effect in the elastic range for this range of wind directions. However, once yield is initiated, the loading on the wires plays a more significant role and the capacity curve for 30° deviates from that for 90° where no load on the wires exists. The relationship of yield capacity and tip displacement at yield for each downburst scenario are shown for each wind direction in Figure 7.

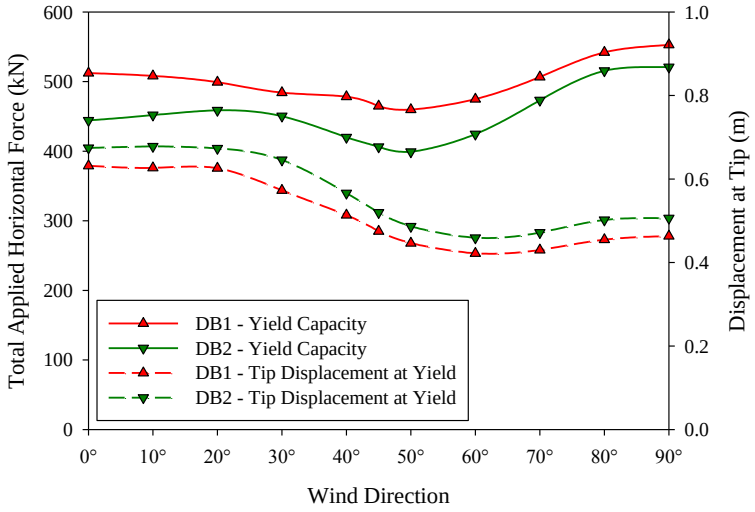

Figure 7. Relationship of yield capacity and tip displacement at yield to wind direction

In general, the capacity curves for DB1 are characterized by greater yield and maximum capacities, and less post-yield deformation. This trend is observed for winds at all directions, with the single exception being for DB2 at 90° where there is a slightly greater maximum capacity than for DB1. It is also shown that there is a greater difference in the capacity curve between wind directions for DB2 than for DB1; this is attributed to the greater loading on the wires for DB2, which results in a loading distribution concentrated in the upper portion of the tower, rather than around mid-height (see wind speed profiles in Figure 3). The capacity curves for each respective downburst scenario have a similar shape, with the exception of wind at 90°, which implies that although the yield capacity varies between wind directions, the tower exhibits similar behaviour in the post-yield range for each wind direction.

To further investigate the effect of downburst size, D_{jet}, on the capacity curve, the analysis is carried out for 250 m < D_{jet} < 1500 m considering the transverse and longitudinal directions only. The obtained capacity curves are shown in Figure 8. It is shown that as the downburst size decreases, the yield capacity of the tower is increased. This can be explained by noting that as the downburst size decreases, the horizontal loads tend to be concentrated at the mid-height of the tower, and the overturning moment is decreased for an equivalent total applied wind load. In other words, for an equal total horizontal wind load, the stress in the structural members is decreased as the downburst size decreases.

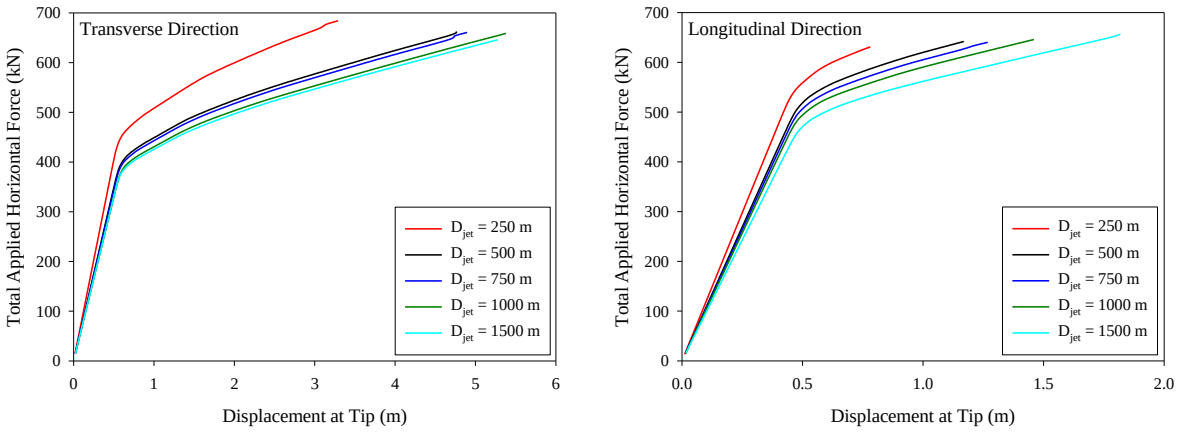

Figure 8. Capacity curves for the transverse and longitudinal wind directions showing variation with D_{jet}

Although no results for capacity curves under ABL or rectangular wind loading are reported here, our experience indicates that the capacity curve for the ABL wind profile serves as an approximate lower bound for the capacity curves associated with downburst wind loads. This is expected, as the wind load due to the ABL wind profile is concentrated on the upper portion of the tower. Furthermore, the capacity curve obtained for the rectangular load profile is likely to serve as an upper bound for the capacity curves associated with downburst wind loads. This can be explained by noting that the use of the rectangular load over the height further increases the load on the lower portion of the tower, at least for D_{jet} > 500 m. A detailed comparison of tower capacity based on the ABL wind profile, rectangular wind profile, and high intensity wind events is to be reported in the near future.

4 Conclusions

The capacity curve of a self-supported lattice transmission tower has been obtained for two downburst scenarios at many orientations relative to the tower using the NSP method. The tower is represented as a 3-D numerical model, and both inelastic material and geometric properties are considered in the analysis. The resulting capacity curves are presented as the force-deformation relationship between the total applied horizontal wind load and the displacement of the tip of the tower. The capacity curves are obtained for two downburst scenarios of different size. The following are key findings from the study:

- The capacity curves for the tower are dependent on the shape of the wind profile. The capacity curves obtained for the downburst scenario characterized by a smaller D_{jet} results in higher yield capacity and less post-yield deformation. The shape of the wind profile has a greater effect on the capacity curve for wind directions where the wires are loaded, due to the load concentration in the upper portion of the tower.
- The shape of the capacity curves for wind directions at which the wires are significantly loaded (i.e., greater than 30°) are quite similar in shape for each respective downburst scenario. The distribution of forces for these directions contributes to a greater amount of post-yield deformation of the tower when compared to wind directions where the wires are not loaded.
- The capacity curves for the tower vary with wind direction, which is primarily due to the asymmetric loading of transmission structures (i.e., the contribution of wind loading on wires). For this particular tower design, the lowest yield capacity for both downburst scenarios are observed for the 45°-50° range of wind direction.
- Multiple downburst sizes (D_{jet}) were investigated for the transverse and longitudinal directions. It is shown that as the downburst size decreases, the horizontal loads tend to be concentrated at the mid-height of the tower rather than the upper portion. Thus, for an equal horizontal wind load, the stress in the structural members is decreased as D_{jet} decreases.

Acknowledgements

The downburst wind fields were made available by Dr. H.M. Hangan of the Boundary Layer Wind Tunnel Laboratory and Department of Civil and Environmental Engineering at the University of Western Ontario. The authors are grateful for many useful discussions with Dr. T.C. Eric Ho over the course of this work. The financial support from the National Sciences and Engineering Research Council of Canada (NSERC) is greatly appreciated.

References

American Society of Civil Engineers (ASCE). 2010. Guidelines for Electrical Transmission Line Structural Loading (3rd edition). *ASCE Manuals and Reports on Engineering Practice No. 74*, Reston, VA.

ANSYS. 2007. ANSYS Multiphysics, Release 9.0, ANSYS Inc., Canonsburg, PA.

Banik, S.S., Hong, H.P. and Kopp, G.A. 2008. Assessment of tornado hazard for spatially distributed systems in southern Ontario. *Journal of Wind Engineering and Industrial Aerodynamics*, **96**(8-9), 1376-1389.

Banik, S.S., Hong, H.P. and Kopp, G.A. 2010. Assessment of capacity curves for transmission line structures under wind loading. *Wind and Structures*, **13**(1), 1-20.

Canadian Standards Association (CSA). 2010. Design Criteria of Overhead Transmission Lines. *CAN/CSA-C22.3 No. 60826-10*, CSA, Toronto, Canada.

Darwish, M.M. and El Damatty, A.A. 2011. Behaviour of self supported transmission line towers under stationary downburst loading. *Wind and Structures*, **14**(5), 481-498.

Durst, C.S. 1960. Wind speeds over short periods of time. *Meteorological Magazine*, **89**, 181-186.

Fujita, T.T. 1985. The Downburst: Microburst and Macroburst. *SMRP Research Paper No. 210*, University of Chicago.

Hangan, H., Roberts, D., Xu, Z. and Kim, J.-D. 2003. Downburst simulations. Experimental and numerical challenges. *Proceedings of the 11th International Conference on Wind Engineering*, Lubbock, TX.

Hangan, H., Savory, E., El Damatty, A., Galsworthy, J. and Miller, C. 2008. Modeling and prediction of failure of transmission lines due to high intensity winds. *Proceedings of the 2008 Structures Congress (ASCE)*, Vancouver, BC.

Kim, J. and Hangan, H. 2007. Numerical simulation of impinging jets wind application to downbursts. *Journal of Wind Engineering and Industrial Aerodynamics*, **95**(4), 279-298.

Krawinkler, H. and Seneviratna, G.D.P.K. 1998. Pros and cons of a pushover analysis of seismic performance evaluation. *Engineering Structures*, **20**(4-6), 452-464.

Lee, P.-S. and McClure, G. 2007. Elastoplastic large deformation analysis of a lattice steel tower structure and comparison with full-scale tests. *Journal of Constructional Steel Research*, **63**(5), 709-717.

Lin, W.E., Savory, E., McIntyre, R.P., Vandelaar, C.S. and King, J.P.C. 2012. The response of an overhead electrical power transmission line to two types of wind forcing. *Journal of Wind Engineering and Industrial Aerodynamics*, **100**(1), 58-69.

Mara, T.G., Galsworthy, J.K. and Savory, E. 2010. Assessment of vertical wind loads on lattice framework with application to thunderstorm winds. *Wind and Structures*, **13**(4), 413-431.

McCarthy, P. and Melsness, M. 1996. Severe weather elements associated with September 5, 1996 hydro tower failures near Grosse Isle, Manitoba, Canada. Environment Canada, Winnipeg, MB.

Orwig, K.D. and Schroeder, J.L. 2007. Near-surface wind characteristics of extreme thunderstorm outflows. Journal of Wind Engineering and Industrial Aerodynamics, **95**(7), 565-584.

Shehata, A.Y. and El Damatty, A.A. 2008. Failure analysis of a transmission tower during a microburst. *Wind and Structures*, **11**(3), 193-208.